Nonsingular quantum gravitational dynamics of an Lemaître-Tolman-Bondi dust shell model: The role of quantization prescriptions

Kristina Giesel,[1,*] Bao-Fei Li,[2,†] and Parampreet Singh[2,‡]

[1]*Institute for Quantum Gravity, Department of Physics, FAU Erlangen-Nürnberg, Staudtstr. 7, 91058 Erlangen, Germany*

[2]*Department of Physics and Astronomy, Louisiana State University, Baton Rouge, Louisiana 70803, USA*

(Received 27 July 2021; accepted 12 November 2021; published 30 November 2021)

We study some consequences of the loop quantization of the outermost dust shell in the Lemaître-Tolman-Bondi spacetime with a homogeneous dust density using different quantization strategies motivated by loop quantum gravity. Prior work has dealt with loop quantizing this model by employing holonomies and the triads, following the procedure in standard loop quantum cosmology. In this work we compare this quantization with the one in which holonomies and gauge-covariant fluxes are used. While both of the quantization schemes resolve the central singularity, they lead to different mass gaps at which a trapped surface forms. This trapped surface which is matched to an exterior generalized Vaidya spacetime disappears when the density of the dust cloud is in the Planck regime. We find that the quantization based on holonomies and gauge-covariant fluxes generically results in an asymmetric evolution of the dust shell in which the Vaidya mass associated with the white hole as seen by an external observer is $2/\pi$ of the one for the black hole. This effective difference in masses results from difference in the classical limits in pre- and postbounce regimes in the two quantizations. This distinctive feature rules out formation of any black-hole-white-hole twins in presence of gauge-covariant flux modifications, which is in contrast to the quantization using holonomies and triads where the gravitational collapse always leads to black hole–white hole twins. Another striking difference lies in the fact that for the quantization based on holonomies and gauge-covariant fluxes there can be situations in which during a nonsingular collapse only a black hole forms without a white hole.

DOI: 10.1103/PhysRevD.104.106017

I. INTRODUCTION

It is generally believed that the singularity problem in the classical gravitational collapse is a consequence of the breakdown of the Einstein theory of general relativity in the Planckian curvature regime and thus can be resolved by quantum gravity. Understanding the role of quantum gravity effects becomes manageable when the collapsing astrophysical body is assumed to be spherically symmetric in which case techniques from canonical quantum gravity can be applied to explore the consequences for singularity resolution and the fate of the spacetime beyond the central singularity. It is expected that a rigorous understanding of quantum gravity effects would also provide insights on fundamental questions related to cosmic censorship conjecture and the black hole evaporation. But to answer these questions, it is important to reliably understand whether the resulting physics is tied to a particular quantization prescription and the way various quantization ambiguities affect the resulting physics of the quantum spacetime and the end state of gravitational collapse.

Loop quantum gravity (LQG) [1–3] is a nonperturbative and background independent approach of quantum gravity which provides a platform for investigating the resolution of the singularities in various situations. In particular, when symmetry reduction is performed before quantization is carried out, loop quantization can in general lead to tractable models which grasp the main features of the quantum gravity corrections to the classical model. For example, a quantization of Friedmann-Lemaître-Robertson-Walker (FLRW) cosmological models using LQG techniques results in loop quantum cosmology (LQC) [4,5], which resolves the big bang singularity by replacing it with a big bounce at the Planck curvature scale [6–8]. While the Hamiltonian constraint in LQC is a difference equation, the underlying dynamics is captured very well by an effective Hamiltonian which indicates a generic resolution of cosmological singularities for isotropic and anisotropic spacetimes [9–14]. These studies have also been generalized to understand the way in which

*kristina.giesel@gravity.fau.de
†baofeili1@lsu.edu
‡psingh@lsu.edu

the above results are robust with respect to some underlying quantization ambiguities such as different choices of the Hamiltonian constraint [15].

Similar to the cosmological setting, within the framework of symmetry reduced LQG, the quantization of black hole spacetimes has been studied in various models using effective spacetime description. For the vacuum spacetimes, most studies are based on the fact that the interior of a Schwarzschild black hole is isometric to the vacuum Kantowski-Sachs spacetime in cosmology. Various quantization schemes, based on holonomies and symmetry reduced triads, have been proposed which result in a generic resolution of the curvature singularity and glue the black hole spacetime to a white hole spacetime through a transition surface [16–26]. Moreover, studies on the vacuum spacetimes have also be extended to include both interior and exterior of the black hole spacetimes [27–33]. On the other hand, investigations have been carried out beyond vacuum spacetimes to include matter such as a massless scalar field (see for e.g., [34–39]). In the classical theory, one of the most studied context is the dust collapse in Lemaître-Tolman-Bondi (LTB) spacetime [40–42], see for instance [43] for an analysis in terms of Dirac observables and [37,44,45] where loop quantum gravitational effects have also been studied. Here the marginally bound case has been well studied when the interior spacetime is isometric to a spatially flat FLRW spacetime for a homogeneous evolution of the dust cloud.[1] These studies have so far focused on exploring the resolution of central singularity using standard techniques in LQC by incorporating quantum geometry effects via holonomies and/or inverse triad modifications [37,45].

Despite this progress, none of the quantizations studied so far for symmetric models has been derived from LQG. Therefore, the robustness of physical predictions from above symmetric models when further modifications from LQG are included in the dynamics remains an important open question. One prominent approach to relate these models to LQG is via coherent states to approximate certain sectors of LQG. But this is challenging for quantizations, as discussed above, which are based on a fixed discretized lattice and flux variables (for a discussion see [49–51]). A resolution is to use gauge-covariant flux variables on a discretized fixed lattice [52]. In this paper our goal is to test the robustness of some of the results obtained in the context of gravitational collapse of the dust cloud using this input from LQG and compare with existing approach based on using holonomies and triads by employing the $\bar{\mu}$ type quantization [7], first for holonomy and triads [7], and then holonomy and gauge-covariant fluxes. This allows us to test some properties of gauge-covariant fluxes in a simpler setup than full LQG where detailed investigations on models involving gauge-covariant fluxes are still an open question. We consider the collapse of a spherically symmetric dust cloud in the marginally bound case assuming that the energy density of the dust cloud is homogeneous so that each shell of the dust cloud collapses at the same relative velocity. As a result, the crossing of the dust shell would never occur during the collapse of the dust cloud and the only relevant singularity in the classical theory is the central singularity when the radius of the dust cloud vanishes.

In this framework we investigate whether different quantization schemes can affect the formation of the trapped horizons and thus lead to distinctive phenomenological signals once the black hole forms during the collapse of the dust cloud. From the numerical simulations of the effective Hamilton's equations, we find that the central singularity is resolved and replaced by a quantum bounce within both quantization schemes. However, there are also distinctive features arising in the second scheme due to the asymmetric evolution of the dust shell. For example, there exists a small region of the parameter space in which a black hole can form during the collapse while a white hole in the expanding stage after the bounce cannot form. Besides, even when both the black hole and the white hole can form in the second scheme, their masses and the duration of the existence of trapped surfaces show qualitatively different behavior from the first scheme. In particular, for generic initial conditions the Vaidya mass of the white hole as seen by an external observer turns out to be $2/\pi$ of the black hole mass. We find that in both the prescriptions there is a mass gap but its value depends on the chosen quantization scheme. These results provide insights on the role of the quantization prescription used in studying the fate of the gravitational collapse using LQG techniques. In particular our results demonstrate in a simple setting that while the resolution of central singularity is a robust feature, the existence of "black hole–white hole" *twins* resulting from the Planck scale physics is not a generic feature. It shows that the resulting physics of loop quantum gravitational collapse can be much richer and complex if further modifications from LQG, than those considered so far, are systematically incorporated.

This paper is organized as follows. In Sec. II, we briefly review the classical LTB dust shell model and derive the classical Hamilton's equations of the outermost shell for the marginally bound case along the lines of [53] using Ashtekar-Barbero variables. We also discuss the criterion for the formation of the trapped surfaces during the collapse of a spherically symmetric object and the matching of the interior of the trapped surface with the exterior spacetimes at the boundary. In Sec. III, we study the effective dynamics of the loop quantization of the dust shell model and employ two quantization prescriptions, the first one only considers the holonomy corrections and the second takes into account both holonomy corrections and gauge covariant fluxes.

[1]See also [46–48] for the bound case whose interior is isometric to a spatially closed FLRW spacetime.

With the help of the numerical analysis of the resulting effective Hamilton's equations, we discuss the phenomenological differences due to the quantization prescriptions. Finally, the main results are summarized in Sec. IV. We use Planck units for numerical simulations and set $\hbar = c = 1$ while keeping Newton's constant G explicit in our formulas.

II. A BRIEF REVIEW OF THE CLASSICAL LTB DUST SHELL MODEL

In this section we briefly review the classical LTB dust model in the canonical framework and write necessary equations using triad and connection variables. The LTB model is obtained from a spherical symmetric solution of Einstein's equations that involve nonrotational dust as the matter source. The metric is given by

$$ds^2 = -d\tau^2 + \frac{(R')^2}{1+2f}dx^2 + R^2 d\Omega^2, \tag{2.1}$$

where we denote the radial coordinate by x, the angular part by $d\Omega^2 = d\theta^2 + \sin^2\theta d\phi^2$ and we have set $c = 1$. $R(x,\tau)$ which is the areal radius of the spherical surfaces is determined by two unknown functions F and f that depend on the radial coordinate and are in turn determined via the following equations

$$8\pi G\rho_{\text{dust}} = \frac{F'}{R^2 R'} \quad \text{and} \quad \dot{R}^2 = \frac{F}{R} + 2f, \tag{2.2}$$

where ρ_{dust} denotes the energy density of the dust and G is Newton's constant. Here $f(x)$ is the total energy of a unit mass at x and $F(x)/2G$ is the active gravitating mass within a sphere with radius $R(x)$. In the so-called marginally bound case one chooses $f = 0$ leading to a simplified form of the metric as well as the LTB equations. We consider the marginally bound case in this work. In the Hamiltonian framework using canonical variables in the Arnowitt-Deser-Misner (ADM) formulation (R, P_R), the Hamiltonian constraints for the gravitational and dust matter sectors have the form

$$H_{\text{grav}} = -\frac{1}{2G}(\dot{R}^2 R)' \quad \text{and} \quad H_{\text{dust}} = \frac{F'}{2G}, \tag{2.3}$$

where $\dot{R}$ is understood as a function of the momentum P_R. Considering the total Hamiltonian constraint $H_{\text{grav}} + H_{\text{dust}} = 0$ then yields the second equation in (2.2).

In order to apply LQG techniques as used in LQC in this context we need to start with a classical LTB model formulated in terms of Ashtekar variables (see for instance [44]). The set of independent canonical variables is given by $(A_x(x), E^x(x))$, $(\gamma K_\varphi(x), E^\varphi(x))$ and a third pair $(\eta(x), P_\eta(x))$ corresponding to the gauge angle, where γ is the Barbero-Immirzi parameter [54,55]. Once the Gauss constraint is implemented the latter pair is eliminated and gauge invariant quantities do not depend on these variables. The relation between the connection variables A_x and the corresponding extrinsic curvature K_x in this case reads $K_x = \frac{1}{\gamma}A_x$. Therefore, the elementary canonical variables satisfy the following Poisson brackets

$$\{K_x(x), E^x(y)\} = 2G\delta(x,y) \quad \text{and}$$
$$\{K_\varphi(x), E^\varphi(y)\} = G\delta(x,y). \tag{2.4}$$

The metric in the marginally bound case in terms of Ashtekar variables can be expressed as

$$ds^2 = -d\tau^2 + \frac{(E^\varphi)^2}{|E^x|}dx^2 + |E^x|d\Omega^2. \tag{2.5}$$

In the ADM case for spherical symmetric models one starts with two sets of variables (R, P_R) and (Λ, P_Λ). For the LTB marginally bound case, as can be seen in (2.1), the metric depends only on R and its derivatives since $\Lambda = R'$ [43]. At the level of Ashtekar variables this results in the following LTB condition

$$E^\varphi(x) = \frac{1}{2}|E^x|'(x). \tag{2.6}$$

As discussed in [44] a second condition relating the two extrinsic curvatures can be obtained by taking the LTB condition in (2.6) as a gauge fixing condition for the diffeomorphism constraint which then yields

$$K'_\varphi = K_x \text{sgn}(E^x). \tag{2.7}$$

The Hamiltonian constraint for the gravitational sector in terms of Ashtekar variables is given by

$$H_{\text{grav}} = -\frac{1}{2G}\left(\frac{K_\varphi^2 E^\varphi}{\sqrt{|E^x|}} + 2K_\varphi K_x\sqrt{|E^x|}\right), \tag{2.8}$$

where at this stage K_φ, E^φ are understood as functionals of K_x, E^x. In order to write down H_{grav} entirely in terms of K_x, E_x one can use the equations of motions for K_φ, E^φ, K_x, E^x to get [44]

$$K_\varphi = \frac{\dot{E}^x}{2\sqrt{|E^x|}} \quad \text{and} \quad K_x = \frac{1}{\sqrt{|E^x|}}\left(\dot{E}^\varphi - \frac{\dot{E}^x E^\varphi}{2E^x}\right). \tag{2.9}$$

If one reinserts these into H_{grav}, then one obtains

$$H_{\text{grav}} = -\frac{1}{2G}\left(\frac{(\dot{E}^x)^2}{4\sqrt{|E^x|}}\right)', \tag{2.10}$$

whereas the dust contribution has again the form $H_{\text{dust}} = \frac{F'}{2G}$. This is consistent with the ADM result (2.3) if one considers the usual relation $R = \sqrt{|E^x|}$.

Now we specialize the LTB model to the shell model. Our strategy is to consider the LTB conditions at the classical level which is sufficient to obtain a model for the outermost shell following the work in [53]. We will briefly summarize the main steps to obtain this model. One of the crucial ingredients of the model is that considering the LTB equations given by

$$8\pi G\rho_{\text{dust}} = \frac{2F'\text{sgn}(E^x)}{\sqrt{|E^x|}(E^x)'} \quad \text{and} \quad (\dot{E}^x)^2 = 4F\sqrt{|E^x|}, \tag{2.11}$$

where the second equation can, as before, be obtained by means of the total Hamiltonian constraint in Ashtekar variables using (2.10). One realizes that the equation for $\dot{E}^x$ only depends on F and E^x but not its spatial derivatives. As a consequence, at the classical level, once a mass function F is chosen the individual shells decouple. The starting point for the outermost shell model in [53] is the Einstein-Hilbert action symmetry reduced to the LTB case plus a boundary term. Next, one notes that the trace of the Einstein-tensor in four dimensions yields $-\mathcal{R}(x)$, where $\mathcal{R}$ denotes the Ricci scalar. Multiplying the trace of the Einstein equations by a volume term then leads to

$$\begin{aligned}\sqrt{|g|}\mathcal{R}(x) &= 8\pi\rho_{\text{dust}}\frac{1}{2}\text{sgn}(E^x)(E^x)'\sqrt{|E^x|}\sin\theta \\ &= \frac{1}{G}F'\sin\theta,\end{aligned} \tag{2.12}$$

where one uses the first LTB equation in (2.11). We denote the radial coordinate of the outermost shell by x_0, then after integrating out the angular part the bulk action has the form

$$\begin{aligned}S_{\mathcal{M}} &= \frac{1}{4G}\int d\tau\int_0^{x_0}F'(x) = \frac{1}{4G}\int d\tau(F(x_0)-F(0)) \\ &= \frac{1}{16G}\int d\tau\frac{(\dot{E}^x)^2(x_0)}{\sqrt{|E^x|(x_0)}},\end{aligned} \tag{2.13}$$

where as in [53] $F(0)=0$ is chosen, meaning that the innermost shell contains no mass. Let us introduce the following compact notation for the quantities of the outermost shell

$$\varepsilon^x := E^x(x_0). \tag{2.14}$$

Using the same boundary term as derived in [53], which in this notation reads $S_{\mathcal{B}} = -\frac{3}{16G}\int d\tau\frac{(\dot{\varepsilon}^x)^2}{\sqrt{|\varepsilon^x|}}$, and adding the bulk and boundary contributions finally, one obtains the full action for the outermost shell of the dust cloud in the LTB model, which reads

$$S = \frac{1}{G}\int d\tau L_{\text{shell}} := -\frac{1}{8G}\int d\tau\frac{(\dot{\varepsilon}^x)^2}{\sqrt{|\varepsilon^x|}}, \tag{2.15}$$

where as in [53] it was used that for Brown-Kuchař dust [56] the action trivially vanishes on shell. Moreover, the triad ε^x and its conjugate momentum k_x, which corresponds to the $1/2$ of the radial component of the extrinsic curvature, satisfy the Poisson bracket

$$\{k_x, \varepsilon^x\} = G, \tag{2.16}$$

then in terms of these canonical variables, the classical Hamiltonian of the outermost shell of the dust cloud takes the form

$$H_{\text{class}} = -\frac{2}{G}k_x^2\sqrt{|\varepsilon^x|} = -M, \tag{2.17}$$

where M stands for the dust mass enclosed by the outermost dust shell. The classical Hamilton's equations can be easily derived from the Hamiltonian with the above Poisson bracket, which explicitly read

$$\dot{\varepsilon}^x = 4k_x\sqrt{|\varepsilon^x|}, \qquad \dot{k}_x = -\frac{k_x^2}{\sqrt{|\varepsilon^x|}}. \tag{2.18}$$

We can rewrite ε^x again in terms of $R(x_0)=R_0$ as $|\varepsilon^x| = R_0^2$ where we suppress the label "0" from now on. The above equations of motion in turn yield the following equations which resemble the classical Friedmann and the Raychaudhuri equations for the areal radius

$$\left(\frac{\dot{R}}{R}\right)^2 = \frac{8\pi G}{3}\rho, \qquad \frac{\ddot{R}}{R} = -\frac{4\pi G}{3}\rho. \tag{2.19}$$

Here ρ denotes the energy density of the dust cloud

$$\rho = \frac{3M}{4\pi R^3}. \tag{2.20}$$

As is well known, the central singularity in the classical theory is inevitable since dynamical equations (2.19) result in the radius of the outermost dust shell to decrease to zero in a finite period of the proper time for a generic set of the initial conditions (R_i, M), where R_i denotes the initial value of the radius. During the collapse of the dust cloud, if a trapped surface can form, then the central singularity will be covered by a horizon. In order to investigate the formation of the trapped surfaces in the interior, it is convenient to introduce two future-directed null vectors normal to the sphere with constant radius, which are [57]

$$\partial_{\xi^+} = \frac{1}{\sqrt{2}}\left(\partial_\tau + \frac{1}{R'}\partial_x\right), \quad \partial_{\xi^-} = \frac{1}{\sqrt{2}}\left(\partial_\tau - \frac{1}{R'}\partial_x\right). \tag{2.21}$$

In the null coordinates ξ^+ and ξ^-, the line element (2.1) (with $f=0$) becomes

$$ds^2 = -2d\xi^+ d\xi^- + R^2 d\Omega^2. \tag{2.22}$$

Hence, we can identify two kinds of the radial null geodesics emerging from the sphere, namely the inward null geodesics $\xi^+ = \text{const}$ and the outward null geodesics $\xi^- = \text{const}$. If the radius decreases along both inward and outward null geodesics, then a trapped surface forms at the sphere. One can introduce the expansion parameter [57]

$$\theta_\pm = \frac{2}{R}\partial_\pm R, \tag{2.23}$$

where $\partial_\pm$ denotes derivatives with respect to $\xi^\pm$, respectively. When the bundles of the light rays converge on both sides of the sphere, $\theta_\pm < 0$, namely $\dot{R} < -1$, then the sphere becomes a future trapped surface corresponding to a black hole. When $\theta_+\theta_- = 0$, the sphere is marginally trapped. On the other hand, if we reverse the directions of the null vectors in (2.21), and then require the bundles of the light rays to converge along these reversed null vectors, which leads to $\dot{R} > 1$, a past trapped surface corresponding to a white hole can form. As a result, in both cases, the trapped surfaces form as long as $\dot{R}^2 > 1$ with the sign of $\dot{R}$ signifying future ($\dot{R} < 0$) or past ($\dot{R} > 0$) directed trapped surface.

While the simplest models of the gravitational collapse, such as Oppenheimer-Snyder-Dutt model, can be recasted as a cosmological model it should be noted that this analogy is only true in the interior of the collapsing object. For a complete picture of a gravitational collapse the interior has to be matched with an exterior spacetime for an external observer. In various situations, with a nonvanishing interior pressure, including for the analysis presented in this paper, the exterior spacetime turns out to be the generalized Vaidya spacetime [58,59], which in the advanced Eddington-Finkelstein coordinates takes the form

$$ds_+^2 = -\left(1 - \frac{2GM(r_v, v)}{r_v}\right)dv^2 - 2dvdr_v + r_v^2 d\Omega^2. \tag{2.24}$$

Here $M(r_v, v)$ is the generic mass function of the Vaidya spacetime which stands for the mass of the black hole if a trapped surface can form during the collapse of the dust cloud. The interior and exterior metrics (2.1) (with $f = 0$) and (2.24) can be matched at the outermost dust shell $x = r_b$ by requiring that the first and second fundamental forms are equal at the boundary. This leads to the following equations:

$$r_v(v)|_\Sigma = R(r_b, t) = r_b a(t), \qquad \left(\frac{dv}{dt}\right)|_\Sigma = \frac{R_{,x} + r_b\dot{a}}{1 - F/R}, \tag{2.25}$$

$$F(t, r_b) = 2M(r_v, v)G, \quad M(r_v, v)_{,r_v}G = \frac{F}{2R} + r_b^2 a\ddot{a}. \tag{2.26}$$

III. EFFECTIVE DYNAMICS OF THE LOOP QUANTIZED LTB DUST SHELL MODEL

In this section, we focus on the evolution of the outermost shell of the dust cloud when the quantum geometric effects motivated from LQG are taken into consideration. Using the techniques of the effective description of the loop quantum dynamics, we loop quantize the outermost shell of the dust cloud and present two effective Hamiltonians resulting from two loop quantizations which yield different physical results. These effective Hamiltonians incorporate the quantum effects at the Planckian energy density and thus successfully resolve the central singularity encountered during the collapse of the classical dust cloud. We then present numerical results from quantum gravity modified dynamical equations and discuss the way initial conditions determine the formation of the trapped horizons during the evolution of the dust shell.

A. Quantum gravity modified dynamical equations

In this subsection, we consider effective dynamics resulting from two loop quantizations of the classical Hamiltonian (2.17). The first is based on using holonomy and triad variables as in standard LQC [7,60], and the second is based on a recently studied quantization of holonomy and gauge-covariant fluxes [49–51]. In addition to the effective Hamiltonian and the equations of motion in each case, we also discuss analytical solutions in the first case and define useful variables for unravelling the dynamics of the collapsing dust cloud through numerical results when analytical solutions are not available.

1. Nonsingular evolution in holonomy and triad quantization

The effective description of the quantum dynamics with the holonomy corrections has been widely corroborated with numerical simulations for both isotropic and anisotropic models in the context of LQC. The modified dynamical equations from the effective Hamiltonian turn out to be an excellent approximation to the underlying quantum dynamics for states which are sharply peaked in a large macroscopic universe [61–64]. Following these investigations, we assume the validity of this approach in our analysis. The marginally bound case corresponds to a spatially flat spacetime in a cosmological setting for which the Ashtekar-Barbero connection is related to extrinsic curvature by a multiplicative constant and the holonomy corrections can be incorporated into an effective Hamiltonian by making the substitution $k_x \to \sin(\delta_x k_x)/\delta_x$ in the classical

Hamiltonian (2.17), here δ_x is known as the polymerization factor which together with k_x determines the regimes where quantum gravity effects become important. On one hand, the quantum geometric effects are manifest in the regime $\delta_x k_x \gg 1$ where the effective dynamics would lead to remarkably distinct predictions as compared with the classical theory. On the other hand, when $\delta_x k_x \ll 1$, the effective Hamiltonian approximates the classical one and the classical theory is recovered in this regime. Moreover, one needs to be careful with the way δ_x depends on or is independent of the phase space variables, otherwise one can get inconsistent infrared regime and fake Planck scale effects. The functional dependence of δ_x on the phase space variables is regarded as polymerization prescriptions. In the spatially flat cosmological setting, there is a unique prescription which is shown to be viable [65], known as improved dynamics (also called $\bar{\mu}$ scheme) [7]. The same prescription has been shown to be a viable one for the nonmarginally bound case too [66]. In this quantization prescription, the dependence of δ_x on the triads is computed by equating the physical area enclosed by honolomy to the minimal eigenvalue of the area operator in LQG, which is $\Delta = 4\sqrt{3}\pi\gamma l_{\rm pl}^2$ [7]. In the following, the Barbero-Immirzi parameter γ is chosen to be 0.2375, which is fixed by the black hole thermodynamics in LQG. To find this relationship we use the correspondence with the cosmological model and note that

$$k_x = \frac{c}{2\gamma}\left(\frac{3}{4\pi}\right)^{1/3}, \qquad \varepsilon^x = p\left(\frac{3}{4\pi}\right)^{2/3}. \tag{3.1}$$

This sets $\delta_x = 2\gamma\lambda/\sqrt{\varepsilon^x}$ with $\lambda = \sqrt{\Delta}$, here we have taken the positive orientation of the triad. As a result, the effective Hamiltonian from the holonomy corrections takes the form

$$H^{\rm hol} = -\frac{(\varepsilon^x)^{3/2}}{2G\lambda^2\gamma^2}\sin^2\left(\frac{2\gamma\lambda k_x}{\sqrt{\varepsilon^x}}\right) = -M, \tag{3.2}$$

where $k_x/\sqrt{\varepsilon^x}$ is proportional to the relative velocity $\dot{R}/R$ of the dust shell in the classical limit. From the effective Hamiltonian (3.2), it is straightforward to show that the equations of motion are

$$\dot{\varepsilon}^x = \frac{\varepsilon^x}{\gamma\lambda}\sin\left(\frac{4\lambda\gamma k_x}{\sqrt{\varepsilon^x}}\right), \tag{3.3}$$

$$\dot{k}_x = \frac{k_x}{2\lambda\gamma}\sin\left(\frac{4\lambda\gamma k_x}{\sqrt{\varepsilon^x}}\right) - \frac{3\sqrt{\varepsilon^x}}{4\gamma^2\lambda^2}\sin^2\left(\frac{2\lambda\gamma k_x}{\sqrt{\varepsilon^x}}\right). \tag{3.4}$$

From the equation of motion (3.3), one can find the following dynamical equation:

$$\left(\frac{\dot{R}}{R}\right)^2 = \frac{8\pi G}{3}\rho\left(1 - \frac{\rho}{\rho_{\rm max}^{\rm hol}}\right), \tag{3.5}$$

where $\rho = \frac{3M}{4\pi R^3}$ and $\rho_{\rm max}^{\rm hol} = 3/(8\pi G\lambda^2\gamma^2)$ denotes the maximum energy density enclosed by the outermost dust shell that is allowed in this model. We see that the quantum geometric effects modify the classical term $8\pi G\rho/3$ with an additional factor which vanishes when the density of the dust cloud becomes equal to $\rho_{\rm max}^{\rm hol}$. Hence, the radius of the dust shell attains its minimum value at the highest energy density and consequently the singularity encountered at $R = 0$ is avoided. Note that the above modified Friedmann equation results in the classical Friedmann equation (2.19) at macroscopic scales both in the prebounce and postbounce phases.

Besides, using the Hamilton's equations (3.3)–(3.4), it is straightforward to show that the energy conservation law in terms of the energy density ρ takes the form

$$\dot{\rho} + 3\frac{\dot{R}}{R}\rho = 0. \tag{3.6}$$

Note that the pressure is defined via $P = -\partial H_m/\partial v$ (with v denoting the volume of the dust cloud) identically vanishes for the effective Hamiltonian (3.2) since $H_m = M$ is a constant.

Similar analysis can be carried out for the $i_{\rm th}$ inner shell of the dust cloud which is labeled by its comoving radius x_i. For such a dust shell, its physical radius is given by $R_i = a(t)x_i$, correspondingly when deriving its Hamiltonian, we only need to integrate along the radial direction from the center of the dust cloud to the comoving radius x_i, resulting in the effective Hamiltonian

$$H^i = -\frac{(\varepsilon^{x_i})^{3/2}}{2G\lambda^2\gamma^2}\sin^2\left(\frac{2\gamma\lambda k_{x_i}}{\sqrt{\varepsilon^{x_i}}}\right) = -\frac{Mx_i^3}{x_{\rm outer}^3}, \tag{3.7}$$

where $\varepsilon^{x_i} = R_i^2$, k_{x_i} is the conjugate momentum of ε^{x_i} and $x_{\rm outer}$ is the comoving radius of the outermost shell. Now starting from the effective Hamiltonian (3.7), one can derive the Hamilton's equations for the $i_{\rm th}$ inner shell in the same way as we did for the outermost shell. It turns out that one can obtain a dynamical equation for the $i_{\rm th}$ shell which has the same form as (3.5) as long as R is replaced with the physical radius of the $i_{\rm th}$ shell R_i. The energy density is still given by $\rho = \frac{3M}{4\pi R^3}$ which is consistent with a homogeneous evolution of the dust cloud. Moreover, since the matter Hamiltonian in (3.7) is a constant for any $i_{\rm th}$ inner shell with a fixed comoving radius x_i, the pressure defined by $p = -\partial H_m/\partial v_i$ (with v_i denoting the physical volume enclosed by the $i_{\rm th}$ inner shell) identically vanishes again and the energy conservation law takes the same form as Eq. (3.6) with R replaced by R_i. Note the energy conservation law (3.6) does not refer to any particular dust shell since $\dot{R}/R = \dot{a}/a$, which is the same for all of the inner shells, therefore any $i_{\rm th}$ dust shell satisfies the same energy conservation law. From the above analysis for the $i_{\rm th}$ inner shell, we conclude that the pressure vanishes identically for any $i_{\rm th}$ dust shell, including the outermost shell of

the dust cloud. As a result, even after loop quantizations, there is still no interactions between neighboring dust shells and we can treat each shell independently from one another.

The quantum gravitational modification in (3.5) can be understood in terms of an "effective energy density" by writing its right-hand side in the same form as in the classical theory. Before going into any details, we want to clarify that quotation marks on "effective energy density," "effective mass" and "effective pressure" in the following are used to emphasize that these effective quantities are not the energy density, mass and pressure from the effective Hamiltonian of the dust shell model but are the quantities which show up in the classical energy momentum tensor when we recast the quantum theory into the form of the classical Einstein's equations. By defining the "effective energy density"

$$\rho_{\rm eff}^{\rm hol} := \rho\left(1-\frac{\rho}{\rho_{\rm max}^{\rm hol}}\right), \tag{3.8}$$

the dynamical equation (3.5) becomes

$$\left(\frac{\dot{R}}{R}\right)^2 = \frac{8\pi G}{3}\rho_{\rm eff}^{\rm hol}. \tag{3.9}$$

Using this "effective energy density" one can also define an "effective mass"

$$M_{\rm eff}^{\rm hol} := \frac{4\pi}{3}R^3\rho_{\rm eff}^{\rm hol}. \tag{3.10}$$

The physical meaning of this "effective mass" $M_{\rm eff}^{\rm hol}$ can be interpreted as follows. Note the Vaidya mass $M(r_v, v)$ is matched with the mass function at the outermost shell of the dust cloud as given in (2.26), namely, $F = 2GM(r_v, v)$. With $F = \dot{R}^2 R$, one can easily find from (3.9) and (3.10) that $F = 2GM_{\rm eff}$. As a result, when the trapped surface forms during the collapse of the dust cloud, the "effective mass" is exactly the mass of the black hole observed by an outside spectator. Same arguments can also be applied to the case in which a white hole forms in the expanding phase of the dust cloud after the bounce. There, the "effective mass" stands for the mass of the white hole as detected by the exterior observer. Finally, the "effective energy density" obeys a conservation law

$$\dot{\rho}_{\rm eff}^{\rm hol} + 3\frac{\dot{R}}{R}(\rho_{\rm eff}^{\rm hol} + p_{\rm eff}^{\rm hol}) = 0. \tag{3.11}$$

with an "effective pressure"

$$p_{\rm eff}^{\rm hol} = -\frac{\dot{M}_{\rm eff}^{\rm hol}}{4\pi R^2\dot{R}}. \tag{3.12}$$

Note although the above "effective pressure" is defined at the boundary, one can analyze the "effective pressure" of the inner shells in a similar way. For the $i_{\rm th}$ inner shell with the comoving radius x_i, we can define the "effective energy density" of the inner shell same as $\rho_{\rm eff}^{\rm hol}$ in (3.8) due to the homogeneous energy density and the corresponding "effective pressure" turns out to be

$$p_{\rm eff}^{i} = -\frac{\dot{M}_{\rm eff}^{i}}{4\pi R_i^2\dot{R}_i} \tag{3.13}$$

with $M_{\rm eff}^{i} := \frac{4\pi}{3}R_i^3\rho_{\rm eff}^{\rm hol}$ denoting the "effective mass" of the $i_{\rm th}$ shell. Now the key observation is that $p_{\rm eff}^{i}$ does not depend on the comoving radius $x_{\rm inner}$. As a result, it is the same for all the shells of the dust cloud, including the outermost shell. Besides, this "effective pressure" is defined according to the "effective energy density" which in turn is defined based on the classical Friedmann equation, any deviations from the classical theory would thus yield a nonzero "effective pressure." However, it should be noted that, in quantum theory, the pressure defined from the effective Hamiltonian (3.7) is still zero for any dust shells. The nonzero "effective pressure" implies a modification of the gravitational sector due to quantum gravity can be compensated by a corresponding modification in the matter sector.

The formation of the trapped surface depends on the magnitude of $\dot{R}^2$ during the collapse of the dust cloud. Specifically, the trapped surface would form if and only if the magnitude of $\dot{R}^2$ becomes greater than unity. This results in a threshold value of the dust mass M^* below which trapped surface does not form. Only when $M > M^*$, a trapped surface would form. On the other hand, if $M < M^*$, no trapped region forms during the collapse of the dust shell.

For the physical Hamiltonian (3.2), one can analytically find the exact expression of M^*. First, from (3.5), it is straightforward to show that

$$\dot{R}^2 = \frac{8\pi G M^{2/3}\rho^{1/3}}{(48\pi^2)^{1/3}}\left(1-\frac{\rho}{\rho_{\rm max}^{\rm hol}}\right). \tag{3.14}$$

Therefore, at $\rho = \rho_{\rm max}^{\rm hol}/4$, $\dot{R}^2$ attains its maximum value which turns out to be

$$\dot{R}_{\rm max}^2 = \frac{3}{4}\left(\frac{GM}{\lambda\gamma}\right)^{2/3}. \tag{3.15}$$

Requiring $\dot{R}_{\rm max}^2 = 1$ yields the threshold value of the dust mass, which is

$$M^* = \frac{8\lambda\gamma}{3\sqrt{3}G} \approx 0.831, \tag{3.16}$$

with $\gamma = 0.2375$ and $\lambda \approx 2.2736$ in Planck units. Moreover, since $\dot{R}^2$ given by (3.14) only depends on the dust mass and the energy density of the dust cloud, the energy density at which the trapped surface forms or vanishes also only depends on the dust mass. In particular, the initial volume does not play any role in determining whether the trapped surface would form during the collapse of the dust cloud.

In addition to the threshold value of the dust mass for the formation of the trapped surface, one can also analytically obtain the time at which the trapped surface forms. Integrating (3.8) leads to

$$R = [2MG\lambda^2\gamma^2 + (\alpha\tau + \beta)^2]^{1/3}, \tag{3.17}$$

where

$$\alpha = -3\sqrt{GM/2}, \qquad \beta = \sqrt{R_i^3 - 2MG\lambda^2\gamma^2}, \tag{3.18}$$

and R_i denotes the initial value of the radius R with the initial time chosen at $\tau_i = 0$. Thus, the bounce happens at $\dot{R} = 0$ when

$$\tau_B = \frac{2\sqrt{R_i^3 - 2MG\lambda^2}}{3\sqrt{2GM}}. \tag{3.19}$$

More features of the dust cloud collapse with holonomy corrections will be discussed through the numerical solutions in the next subsection.

Before moving onto the second quantization ansatz, we would like to emphasize that the quantization of the homogeneous evolution of the dust cloud in this subsection is carried out based on the classical Hamiltonian constraint (2.17) which comes from applying the classical LTB conditions to the gravitational sector of the Hamiltonian constraint given by (2.8) in the spherically symmetric phase space. Consequently, the classical LTB conditions are also implicitly satisfied for the effective dynamics prescribed by the effective Hamiltonian constraint (3.2). At a first sight, this seems contradictory to the results given in [44] in which the authors showed explicitly the modifications to the classical LTB conditions due to the quantum gravity effects. However, it should be noted that those modifications are also due to an inhomogeneous evolution of the dust cloud. Here we note that a recent work in [25] loop quantizes the spherically symmetry reduced phase space starting from the classical gravitational Hamiltonian (2.8). In [25], the authors derived a full set of the equations of motion for E^φ, E^x and their conjugate momenta by using the effective dynamics which constitute a closed set of partial differential equations [see Eqs. (4.1)–(4.4) in [25]]. It can be shown that for the homogeneous evolution of the dust cloud, equations of motion in [25] are consistent with the classical LTB conditions and result in the Eqs. (3.3) and (3.4). As a result, solutions discussed in this subsection agree with those obtained from the homogeneous reduction of the full set of the equations of motion without assuming the homogeneity of the interior spacetime. One can regard our model as the simplest case which only focuses on the quantum geometrical effects on the resolution of the classical singularity and and the formation of the trapped surfaces. In particular, no interactions between the neighboring shells of the dust cloud are taken into account. To consider more complicated situations, one needs to refer to the full set of the equations of motion (4.1)–(4.4) in [25] where an inhomogeneous evolution of the dust cloud is certainly expected to incorporate the interactions between the shells and thus change the dynamics of the outermost shell.

2. Nonsingular evolution in holonomy and gauge-covariant flux quantization

So far we have considered loop quantum gravity effects using holonomies of the connection and *symmetry reduced triads*. The usage of triads, instead of fluxes, is possible because of symmetry reduction. While this strategy works for the loop quantization of symmetry reduced models, one needs to go beyond this approach if one wishes to obtain an effective Hamiltonian with loop quantum modifications from loop quantum gravity using suitable coherent states. A possibility in this direction requires an introduction of *gauge-covariant fluxes*, first introduced by Thiemann [52], which have been recently implemented in loop quantization of cosmological spacetimes [49–51]. It turns out that the corresponding quantum effects can be incorporated into the effective Hamiltonian by making the substitution $\sqrt{\varepsilon^x} \to \sqrt{\varepsilon^x}\mathrm{sinc}(\delta_x k_x/2)$ in the classical Hamiltonian (2.17), which, together with the holonomy corrections in k_x, gives rise to the following effective Hamiltonian:

$$H^{\mathrm{g.c.}} = -\frac{(\varepsilon^x)^{3/2}}{2G\gamma^2\lambda^2}\sin^2\left(\frac{2\lambda\gamma k_x}{\sqrt{\varepsilon^x}}\right)\mathrm{sinc}\left(\frac{\gamma\lambda k_x}{\sqrt{\varepsilon^x}}\right) = -M. \tag{3.20}$$

To distinguish this effective Hamiltonian from the one where only holonomy modifications were incorporated, we label it with superscript "g.c." for inclusion of gauge-covariant flux modifications in addition to holonomy modifications.

Correspondingly, the equations of motion in this case are given by

$$\dot{\varepsilon}^x = \frac{(\varepsilon^x)^{3/2}}{2\lambda^2\gamma^2 k_x}\sin\left(\frac{2\gamma\lambda k_x}{\sqrt{\varepsilon^x}}\right)\sin\left(\frac{\lambda\gamma k_x}{\sqrt{\varepsilon^x}}\right) \times\left\{1 + 5\cos\left(\frac{2\gamma\lambda k_x}{\sqrt{\varepsilon^x}}\right) - \frac{\sqrt{\varepsilon^x}}{\gamma\lambda k_x}\sin\left(\frac{2\gamma\lambda k_x}{\sqrt{\varepsilon^x}}\right)\right\}, \tag{3.21}$$

$$\dot{k}_x = \frac{\sqrt{\varepsilon^x}}{4\lambda^2\gamma^2}\sin\left(\frac{2\gamma\lambda k_x}{\sqrt{\varepsilon^x}}\right)\sin\left(\frac{\gamma\lambda k_x}{\sqrt{\varepsilon^x}}\right) \times\left\{1+5\cos\left(\frac{2\gamma\lambda k_x}{\sqrt{\varepsilon^x}}\right)-4\frac{\sqrt{\varepsilon^x}}{\lambda\gamma k_x}\sin\left(\frac{2\gamma\lambda k_x}{\sqrt{\varepsilon^x}}\right)\right\}. \quad (3.22)$$

The classical equations of motion (2.18) can be recovered from the above equations in the limit when $k_x/\sqrt{\varepsilon^x} \ll 1$. While the above dynamical equations result in a nonsingular bounce as in standard LQC, there are some key differences in the evolution. In particular, in presence of gauge-covariant fluxes matter acts nonminimally coupled and the bounce turns out to be generically asymmetric [50,51].

In the case with the gauge covariant fluxes, a closed form of the modified Friedmann equation analogous to (3.8) is not available. As a result, an analytical analysis of the threshold value of the dust mass for the formation of the trapped horizon is not possible. However, one can use the numerical simulations to understand the dynamics of the collapse of the dust cloud in this model by using the criteria for the formation of a trapped surface which is still given by $\dot{R}^2 \geq 1$. Besides, the asymptotic form of the Friedmann equation can be obtained from the large volume approximation as what has been done for a massless scalar field in [50]. Due to the nonminimal coupling of the matter sector with gravity, the asymptotic form of the Friedmann equation also changes with the equation of state of the matter content. For the dust field, following the similar calculations in [50], it is straightforward to show that in the collapsing phase of the dust cloud, the asymptotic form of the Friedmann equation assumes

$$H^2|_{\text{collapse}} = \frac{8\pi G}{3}\rho + \mathcal{O}(\rho^2), \quad (3.23)$$

while the asymptotic form of the Friedmann equation in the expanding phase of the dust cloud reads

$$H^2|_{\text{expanding}} = \frac{8\pi\alpha G}{3}\rho + \mathcal{O}(\rho^{3/2}), \quad (3.24)$$

with $\alpha = 2/\pi$.[2] The origin of this α in holonomy-gauge-covariant flux modifications is tied to the "sinc" term in the Hamiltonian. Note that in both quantizations, the postbounce classical branch corresponds to $|2\gamma k_x/\sqrt{\varepsilon^x}|$ reaching π/λ. In standard quantization based on holonomies and triads this is indistinguishable from the prebounce classical branch $2\gamma k_x/\sqrt{\varepsilon^x} \approx 0$. The prebounce and postbounce branches in this quantization are thus identical in the classical limit. However, the sinc term in the presence of gauge covariant flux modifications results in *different* classical limits in the prebounce and postbounce epochs. These branches though still correspond to Friedmann dynamics, they have difference due to above α scaling, which is the cause of asymmetry in the "effective mass" of the white hole as seen by an external observer.

Now following (3.9), one can define the same "effective energy density" and the "effective mass," namely,

$$\rho_{\text{eff}} := \frac{3}{8\pi G}\frac{\dot{R}^2}{R^2}, \qquad M_{\text{eff}} := \frac{4\pi}{3}R^3\rho_{\text{eff}}. \quad (3.25)$$

The "effective energy density" ρ_{eff} determines the relative collapsing (expanding) speed of the dust outermost shell, while the effective mass M_{eff} which is the same as the Vaidya mass determines the mass of the black hole (during the collapsing phase) or the white hole (during the expanding phase) if trapped surfaces are formed. When the volume is macroscopic and energy density is far below the Planck scale, using (3.23), we find during the collapse of the dust cloud

$$M_{\text{eff}}|_{\text{collapse}} = \frac{R^3}{2G}H^2|_{\text{collapse}} \approx \frac{4\pi}{3}R^3\rho = M. \quad (3.26)$$

Therefore, initially the "effective mass" is equal to the mass of the dust cloud. On the other hand, after the bounce, when the dust cloud expands to a low energy density $\rho(\ll \rho_{\text{pl}})$, using (3.24), one can easily find

$$M_{\text{eff}}|_{\text{expanding}} = \frac{R^3}{2G}H^2|_{\text{expanding}} \approx \frac{4\pi\alpha}{3}R^3\rho = \alpha M, \quad (3.27)$$

which implies that, after the bounce, the "effective mass" of the dust cloud is just a fractional of the initial mass from the perspective of an outside observer. The same argument also applies to the case when the trapped surface forms, leading to a black hole and white hole asymmetry. Accompanied with the "effective energy density," one can also define an "effective pressure" via

$$p_{\text{eff}} = -\frac{\dot{M}_{\text{eff}}}{4\pi R^2\dot{R}}, \quad (3.28)$$

which satisfies

$$\dot{\rho}_{\text{eff}} + 3\frac{\dot{R}}{R}(\rho_{\text{eff}} + p_{\text{eff}}) = 0. \quad (3.29)$$

Note that in the classical theory, M_{eff} equals M and thus $p_{\text{eff}} = 0$ which is consistent with the fact that the matter content only consists of dust. However, in a model with quantum corrections, whether originating from just holonomies or holonomies and gauge-covariant fluxes, M_{eff} is in general time dependent and p_{eff} becomes nonzero. For this reason it is necessary to match the interior quantum modified spacetime with a generalized Vaidya spacetime.

[2]This additional factor α can also be absorbed into the Newton's constant, yielding a rescaled Newton's constant $\tilde{G} = \alpha G$.

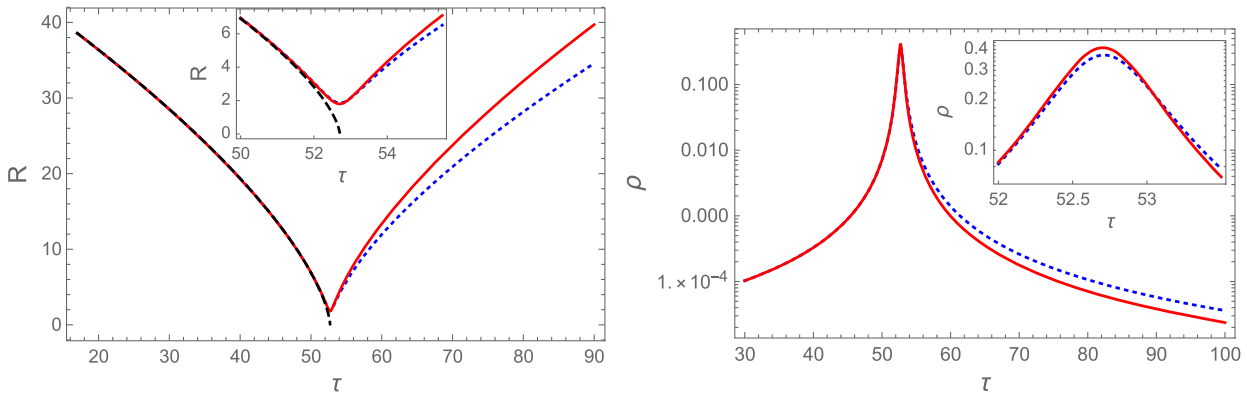

FIG. 1. With the initial conditions $R_i = 50$, $M = 10$, the classical trajectory of R (black dashed) is compared with those from the effective dynamics prescribed by holonomy-triad quantization (3.2) (red solid) and holonomy-gauge-covariant flux quantization (3.20) (blue dotted) in the left panel. In the inset plot, it can be seen that the classical trajectory (black dashed curve) ends at the singularity point when $R = 0$, while in the other two trajectories a bounce occurs at nonzero radius. In the right panel, we can find the difference in the energy densities of two loop quantized models mainly in the expanding branch. The inset plot shows the difference of the maximum energy densities in the two models. All values are in Planck units.

Finally, it is important to note that the different "effective masses" in the collapsing and expanding phases does not imply the violation of the energy conservation law. The change in the "effective mass" is completely due to the quantum modifications in the gravitational sector of the Hamiltonian constraint. The matter sector of the Hamiltonian constraint remains untouched as can be seen by comparing the classical Hamiltonian (2.17) and the effective Hamiltonian (3.20). As a result, the energy density of the dust cloud still evolves according to $\rho = \frac{3M}{4\pi R^3}$ in both collapsing and expanding phases and the conservation law $\dot{\rho} + 3H\rho = 0$ always holds. Moreover, even in terms of the "effective energy density" and the "effective pressure," the energy conservation law (3.29) holds for both branches.

B. Numerical results of the effective dynamics

We now present numerical results for the effective dynamics of the loop quantized dust outermost shell in the marginally bound case and compare the distinctive features resulting from the Hamiltonians (3.2) and (3.20). For convenience, the first model with only holonomy corrections is called model A and the second model, which is quantized by employing both holonomies and gauge covariant fluxes, is called model B. Without any loss of generality, we set the initial time at $\tau = 0$. The parameter space consists of the initial values of the radius R_i and the dust mass M. We find that for a generic set of the initial conditions (R_i, M), the singularity point at $R = 0$ is replaced by a bounce in both models, but with important differences in the physics of the bounce and postbounce dynamics. Before the bounce, the dust cloud collapses in a contracting phase, and after the bounce the dust cloud keeps expanding toward infinity.

In Fig. 1, we show a representative case with $R_i = 50$ and $M = 10$ (in Planck units). The left panel depicts the evolution of the radius R of the shell in the classical theory (black dashed curve), in model A with holonomy corrections (red solid curve) and in model B with both holonomies and gauge covariant fluxes (blue dotted curve). In the classical theory, the radius becomes zero at a finite proper time while in models A and B, the radius of the shell experiences a bounce at the maximum energy density and the dust shell enters into an expanding phase afterwards. The bounce in both models takes place at around $\tau \approx 52.70$ (in Planck units). The difference between two loop quantized models mainly lies in the expanding phase and they also have different maximum energy densities. In model A, the evolution is symmetric with respect to the bounce while in model B, we observe an asymmetric bounce due to the gauge covariant fluxes. Starting with the same initial conditions, the expansion rate of the dust cloud in model B is smaller than that in model A. Besides, the maximum energy density in model A is $\rho_{\max}^{\mathrm{hol}} \approx 0.409$, while in model B the maximum energy density is $\rho_{\max}^{\mathrm{g.c.}} \approx 0.370$ in Planck units.

We find for both models, the formation of a trapped surface does not depend on the initial values of the radius which would only affect the bounce time. The only parameter that affects the formation of the trapped surface is the dust mass M. Moreover, we observe different patterns in two loop quantized models which are summarized in Fig. 2. In the figure, we present the $\dot{R}^2$ plot for both models. The left panel is for model A and the right panel is for model B. As discussed in the last subsection, in the contracting phase when the dust cloud collapses, the black hole forms in the period when $\dot{R}^2 > 1$. On the other hand, a white hole would form if $\dot{R}^2$ becomes larger than unity again in the expanding phase after the bounce. In model A (left panel), the peaks of $\dot{R}^2$ are symmetric with respect to the bounce. This shows that if the contracting branch

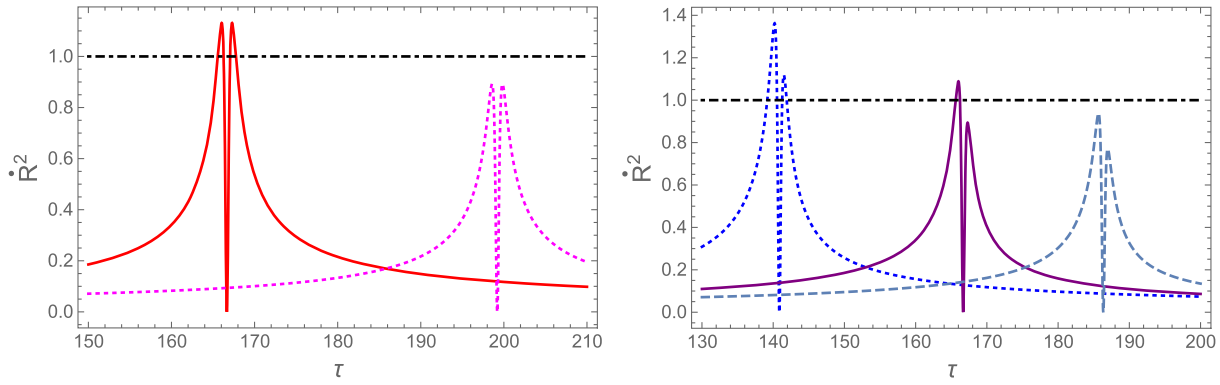

FIG. 2. With the fixed initial radius $R_i = 50$, we change the dust mass M in both of the models to show the effects of the dust mass on the formation of the trapped surfaces corresponding to black hole (white hole) before (after) the bounce point. In the left panel, the dust mass is set to $M = 1.0$ (red solid) and $M = 0.7$ (magenta dotted) in the first model with only holonomy corrections. In the right panel, the dust mass from left to right is set, respectively, to $M = 1.4$ (blue dotted), $M = 1.0$ (purple solid) and $M = 0.8$ (dashed) in the second model which also considers the gauge covariant flux. The trapped horizon forms when $\dot{R}^2 \geq 1$.

produces a black hole then the expanding branch produces its twin white hole. There is a threshold value of the dust mass which determines whether black hole or white hole would form. Its analytic value $M^* \approx 0.831$ given in (3.16) exactly matches with our numerical results. In particular, our numerical investigations for masses below this threshold did not find formation of a trapped surface. In the figure, we show two cases with $M = 1.0$ and $M = 0.7$. In the former case, a black (white) hole forms near the bounce, while, in the latter case, neither a black hole nor a white hole would form during the entire evolution. Finally, once the dust mass is fixed, from Eq. (3.14) one can deduce at what energy density the trapped surfaces would form or vanish. In the case of $M = 1.0$, we find that during the collapse of the dust cloud, the black hole forms at $\rho = 0.041$ and evaporates at $\rho = 0.188$. Owing to the symmetric bounce, when the dust cloud enters into the expanding phase after the bounce, the white hole would form at $\rho = 0.188$ and vanish at $\rho = 0.041$. Increasing the dust mass would decrease/increase the energy densities at which the trapped surfaces form/vanish during the collapsing phase of the dust cloud. For example, when $M = 2000$, the black hole would form at $\rho = 7.460 \times 10^{-9}$ and then evaporate at $\rho = 0.408$. As $\dot{R}^2$ changes monotonically with the dust mass in (3.14), the energy density at which the trapped surfaces form or vanish also changes monotonically with the dust mass.

The situation becomes richer for model B (right panel in Fig. 2) where we find that $\dot{R}^2$ is asymmetric with respect to the bounce point. As a result, there are two characteristic dust masses $M_1 = 0.880$ and $M_2 = 1.184$. When the dust mass $M < M_1$, there would be no black hole or white hole as depicted by the rightmost dashed curve in the right panel. When $M_1 < M < M_2$, only the black hole can form during the collapse of the dust cloud, there would be no white hole in the expanding phase. This case corresponds to the one depicted by the middle purple solid curve in the right panel. Lastly, if $M > M_2$, then both a black hole and a white hole can form as depicted by the blue dot-dashed curve. Since the closed forms of the dynamical equations which yield an analytical value of mass threshold are not available for this model, the above threshold values of the dust mass for the formation of the black hole and white hole are determined numerically. We have checked with various different initial radii and find the same threshold values of the dust mass. Moreover, given a specific dust mass, one can only find the energy densities at which the black hole and the white hole would form and vanish through the numerical solutions. In the case mentioned in the right panel of Fig. 2, we find for $M = 1.4$, the black hole would form at $\rho = 0.0126$ and evaporate at $\rho = 0.154$. Correspondingly, the white hole would form at $\rho = 0.130$ and vanish at $\rho = 0.0364$. One can also increase the dust mass and find the similar patterns as in model A with only holonomy corrections. For example, when $M = 2000$, the black hole would form at $\rho = 2.98 \times 10^{-8}$ and evaporate at $\rho = 0.368534$ while the corresponding white hole would form at $\rho \approx 0.368517$ and vanish at $\rho = 1.16 \times 10^{-7}$. We find that the formation of trapped surfaces does not depend on the initial radius. Note that there also exists an asymmetry in the energy densities for the formation or the evaporation of the black hole and the white hole in model B. Thus we find a key difference between the physics of model A and B. Contrary to the model where triads and holonomies are used, in presence of gauge-covariant flux modifications a black hole–white hole twin system is not possible and there can be situations where only a black hole forms.

In addition, we also find the difference in the "effective masses" between two models. In Fig. 3, we choose the initial conditions $R_i = 2500$, $M = 1000$ (in Planck units) so that both black hole and the white hole will form in the two considered models. From the figure, one can find

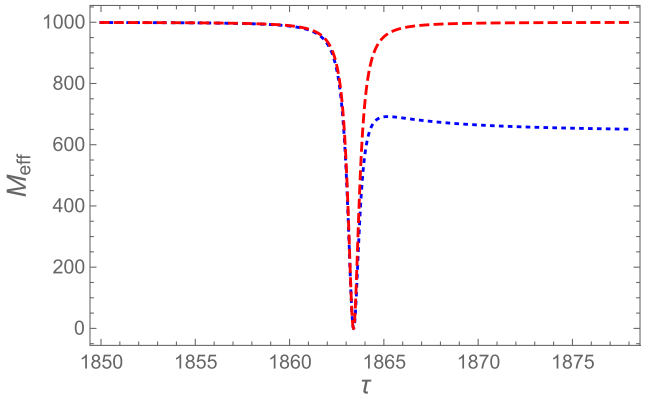

FIG. 3. With the initial conditions $R_i = 2500$, $M = 1000$, the "effective mass" in two models are compared near the bounce. The difference between two models exhibits itself in the expanding phase where the red dashed curve returns to its initial value quickly after the bounce while the blue dotted curve can only return to $2/\pi$ of its original value.

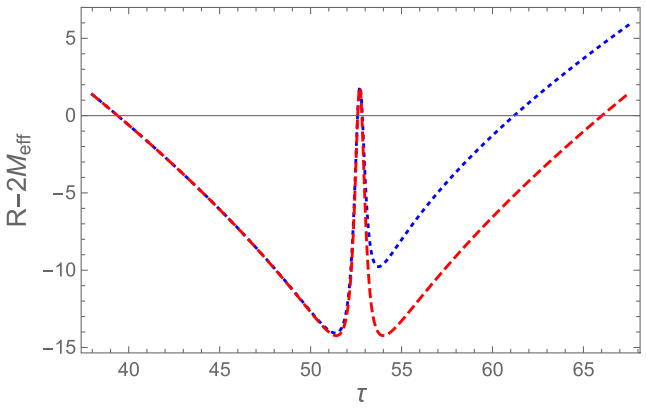

FIG. 4. With the initial conditions $R_i = 50$, $M = 10$, we show explicitly the evolution of the trapped horizon near the bounce. The bounce takes place at the peak in the middle of the plot. The red dashed curve is for model A with only the holonomy corrections while the blue dotted curve is for model B, which also considers gauge covariant fluxes.

initially when the quantum gravity effects can be ignored, the "effective mass" is equal to the dust mass in both cases. As the dust cloud continues to collapse, the "effective mass" drops slowly initially. It is only near the bounce that the "effective mass" starts to change drastically. Right at the bounce, the "effective mass" vanishes, which implies, for an exterior observer, that the spacetime reduces to the flat Minkowski spacetime at the bounce. The remarkable difference between two models takes place in the expanding phase. In model A (red dashed curve), the dust cloud can return to its initial configuration with a reversed velocity, as the quantum gravity effects disappear, the "effective mass" also returns to its initial value. However, in model B with modifications from the gauge covariant fluxes, the "effective mass" can only at most return to about $\alpha M \approx 636.62$, which is exactly given by our analytical predictions in (3.27). Finally, since the $M_{\rm eff}$ is asymmetric with respect to the bounce in model B, the masses of the black hole and the white hole also evolve asymmetrically with respect to the bounce.

As the "effective mass" $M_{\rm eff}$ equals the mass of the black hole and white hole once the trapped surface is formed, one can also track the formation of the trapped surface using the $(R - 2M_{\rm eff})$ plot. We give such an example in Fig. 4 with the initial conditions $R_i = 50$, $M = 10$. The black hole and the white hole are formed when $R < 2M_{\rm eff}$. The central maximum at around $t \approx 52.70$ in the plot corresponds to the bounce point. From the figure, we can clearly see when the trapped surface forms and disappears in both of the models. When the dust cloud is in the collapsing phase, the radius decreases faster than the "effective mass." The trapped surface forms in the regime $39.39 < t < 52.58$ for which $R < 2M_{\rm eff}$ and disappears in the interval $52.58 < t < 58.84$ when $R > 2M_{\rm eff}$. Right at the bounce $t \approx 52.70$, $M_{\rm eff}$ vanishes and $(R - 2M_{\rm eff})$ attains its local maximum. After the bounce, in order to form a trapped surface during the expanding phase, $2M_{\rm eff}$ which equals zero at the bounce has to increase more quickly than R so that $(R - 2M_{\rm eff})$ becomes negative again at some instant of time (in the current case, this time is $t \approx 58.84$ for both models). In this expanding branch, the difference between the two models exhibits itself in terms of the duration of the trapped surfaces. To be specific, in model A (red dashed curve) which includes only holonomy corrections, the trapped surface forms at around $t \approx 58.84$ and disappears at around $t \approx 66.02$ while in model B (blue dotted curve), which includes quantum effects from holonomy corrections and the gauge covariant fluxes, the trapped surface lasts from $t \approx 58.84$ to $t \approx 61.19$. As a result, in model A, the black hole and white hole have the same "lifetime" in terms of the proper time τ, while in model B, the black hole outlives the white hole in the proper time τ.

While there are qualitative differences between the two models, the behavior of the "effective energy density" and the violation of the weak energy conditions when measured with respect to "effective energy densities" in the two models is similar. In Fig. 5, we present a typical evolution of the "effective energy density" in both models with the initial conditions $R_i = 50$, $M = 10$. One can find two models share the similar behavior: as the dust cloud collapses, the "effective energy density" initially increases until its maximum value before the bounce then it decreases rapidly. At the bounce, the "effective energy density" vanishes which implies that an outside observer can only see an asymptotic flat Minkowski spacetime at the bounce. Afterwards, the "effective energy densities" increases again to its maximum as the dust cloud starts to expand. This results in the formation of the white hole in the expanding phase when $R < 2M_{\rm eff}$. As the radius keeps increasing, the "effective energy density" would finally decrease. Finally,

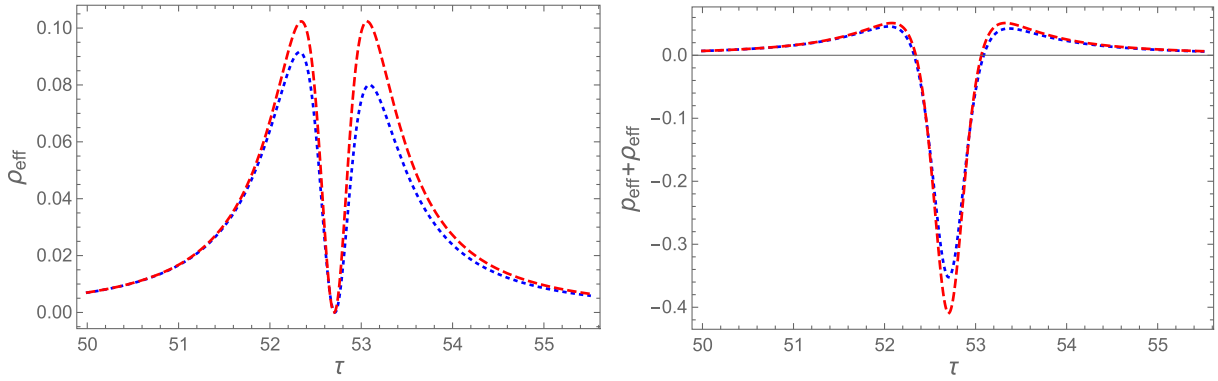

FIG. 5. With the initial conditions $R_i = 50$, $M = 10$, apart from some quantitative differences, the "effective energy density" in model A (red dashed curves) and model B (blue dotted curves) have the similar behavior. In particular, the "effective energy densities" vanish at the bounce and the weak energy condition is violated in a neighborhood of the bounce.

in the right panel, we can find near the bounce between $\tau \approx 52.32$ and $\tau \approx 53.09$, the weak energy condition in terms of the effective density and pressure is violated in both models.

It is important to note that the above qualitative differences and similarities between the two models are robust with respect to the change in the dust mass and the initial radius of the dust cloud. In particular, the symmetric bounce in model A and asymmetric bounce in model B, the threshold values of the dust mass for the formation of the trapped surfaces in both models, as well as the black hole and white hole symmetry (asymmetry) in model A (B) are the properties of models independent of the specific choices of the initial conditions and were found to hold for a large range of values of mass parameter.

IV. CONCLUSIONS

In this paper, we have studied and compared the dynamical consequences of two loop quantizations of the dust shell model. The first quantization uses the holonomies and triads while the second quantization employs the holonomies and the gauge covariant fluxes. Note that in standard LQC the use of triads follows because of the symmetry reduction and homogeneity. On the other hand the motivation to use gauge-covariant fluxes arises from treating holonomies and fluxes at a similar level during quantization in LQG [52] and to obtain the effective Hamiltonian in LQC as an expectation value of the scalar constraint operator using suitable coherent states in LQG. In the classical dust shell model, we assume the LTB dust spacetime with marginally bound condition so that the initial dust velocity at spatial infinity vanishes. Moreover, we also assume a homogeneous dust density so that all shells of the dust cloud collapse and expand at the same rate. In this way, there is no shell crossing singularity and all of the shells reach the central singularity at $R = 0$ simultaneously. In both of the loop quantized models, the said central singularity is resolved for a generic set of the initial conditions for the collapsing dust cloud. The dust shell bounces back after some period of collapse when the maximum energy density allowed in each model is reached. Afterwards, the dust cloud keeps expanding until all the matter is radiated to infinity.

Besides the generic resolution of the central singularity, in both models, the formation of the trapped surfaces only depends on the dust mass M. However, there are important qualitative distinctions in the dynamics of two loop quantized models. In the first model with only holonomy corrections, the evolution of the radius, the velocity of the dust shell, the "effective mass" and the "effective energy density" is symmetric with respect to the bounce point, while in the second model with both holonomy corrections and modifications from the gauge covariant fluxes, the evolution of the corresponding variables become asymmetric with respect to the bounce. The symmetric/asymmetric bounce results in the following physical consequences. In the first model, we find a threshold value of the dust mass M^* below which no trapped surface would form during the entire evolution of the dust cloud. It is only when the dust mass is larger than M^* that the trapped surfaces could then form on both sides of the bounce. The trapped surface which forms during the collapse of the dust cloud corresponds to a dynamical black hole while the trapped surface which forms during the expansion of the dust cloud after the bounce is a dynamical white hole. The black hole and the white hole lie symmetrically on both sides of the bounce point. Between them is an asymptotic flat Minkowski spacetime, owing to the vanishing "effective mass" ("effective energy density") at the bounce point.

On the other hand, in the second model which includes gauge-covariant flux modifications, we find a much richer situation. In contrast to the first model, the formation of the black hole in the collapsing phase does not guarantee the formation of the white hole in the expanding phase. There actually exist two characteristic dust masses M_1 and M_2 ($M_1 < M_2$). When the mass of shell is less than M_1, neither black hole nor white hole would form during the collapse or

the expansion of the dust cloud. When the dust mass lies between M_1 and M_2, only the black hole can form during the collapse of the dust cloud. Finally, when the dust mass is larger than M_2, both a black hole and a white hole can form on different sides of the bounce point. For the last case, unlike in the first model, the evolution of the black and the white hole is not symmetric with respect to the bounce point.

Another remarkable difference between two loop quantized models lies in the behavior of the "effective mass" and the duration of the trapped surfaces in two models. In the first model with only holonomy corrections, the "effective mass" evolves symmetrically with respect to the bounce. It tends to the same dust mass on both sides of the bounce when the dust energy density approaches zero. However, in the second model, the asymptotic value of the "effective mass" of the dust cloud in the expanding phase is only $2/\pi$ of its initial value in the collapsing phase. As the "effective mass" remains almost constant in most of the times of the evolution and it only changes drastically near the bounce, this asymmetry can also be interpreted as the asymmetry in the masses of the black hole and white hole formed during the collapse and the expanding phases, respectively. Moreover, in the first model, the black hole and the white hole have the same lifetime in terms of the proper time τ while, in the second model, the black hole outlives the white hole as a consequence of the asymmetric bounce which is a unique feature of the second model. In summary, our results show that various aspects of the black hole–white hole symmetry which exists in models based on holonomy modifications are nonexistent when one also includes gauge-covariant flux modifications motivated by loop quantum gravity. Further, our analysis shows that even for the simplest situation of the marginally bound case different quantization prescriptions can result in qualitatively different physics for the white hole spacetime.

ACKNOWLEDGMENTS

We are grateful to the anonymous referee for valuable comments. We also thank Jahnvi Verma and Anzhong Wang for comments on the manuscript. This work is supported by the DFG-NSF Grants No. PHY-1912274, No. 425333893, No. PHY-1454832, and No. PHY-2110207.

[1] C. Rovelli, Loop quantum gravity, Living Rev. Relativity **1**, 1 (1998).
[2] A. Ashtekar and J. Lewandowski, Background independent quantum gravity: A status report, Classical Quant. Grav. **21**, R53 (2004).
[3] T. Thiemann, *Introduction to Modern Canonical Quantum General Relativity* (Cambridge University Press, Cambridge, England, 2007).
[4] A. Ashtekar and P. Singh, Loop quantum cosmology: A status report, Classical Quant. Grav. **28**, 213001 (2011).
[5] I. Agullo and P. Singh, *Loop Quantum Cosmology, in Loop Quantum Gravity: The First 30 Years*, Edited by A. Ashtekar and J. Pullin (World Scientific, Singapore, 2017).
[6] A. Ashtekar, T. Pawlowski, and P. Singh, Quantum Nature of the Big Bang, Phys. Rev. Lett. **96**, 141301 (2006).
[7] A. Ashtekar, T. Pawlowski, and P. Singh, Quantum nature of the big bang: Improved dynamics, Phys. Rev. D **74**, 084003 (2006).
[8] A. Ashtekar, A. Corichi, and P. Singh, Robustness of key features of loop quantum cosmology, Phys. Rev. D **77**, 024046 (2008).
[9] P. Singh, Are loop quantum cosmos never singular?, Classical Quant. Grav. **26**, 125005 (2009).
[10] P. Singh and F. Vidotto, Exotic singularities and spatially curved loop quantum cosmology, Phys. Rev. D **83**, 064027 (2011).
[11] P. Singh, Curvature invariants, geodesics and the strength of singularities in Bianchi-I loop quantum cosmology, Phys. Rev. D **85**, 104011 (2012).
[12] S. Saini and P. Singh, Geodesic completeness and the lack of strong singularities in effective loop quantum Kantowski-Sachs spacetime, Classical Quant. Grav. **33**, 245019 (2016).
[13] S. Saini and P. Singh, Resolution of strong singularities and geodesic completeness in loop quantum Bianchi-II spacetimes, Classical Quant. Grav. **34**, 235006 (2017).
[14] S. Saini and P. Singh, Generic absence of strong singularities in loop quantum Bianchi-IX spacetimes, Classical Quant. Grav. **35**, 065014 (2018).
[15] S. Saini and P. Singh, Generic absence of strong singularities and geodesic completeness in modified loop quantum cosmologies, Classical Quant. Grav. **36**, 105014 (2019).
[16] A. Ashtekar and M. Bojowald, Quantum geometry and the Schwarzschild singularity, Classical Quant. Grav. **23**, 391 (2006).
[17] L. Modesto, Loop quantum black hole, Classical Quant. Grav. **23**, 5587 (2006).
[18] C. G. Bohmer and K. Vandersloot, Loop quantum dynamics of the Schwarzschild interior, Phys. Rev. D **76**, 104030 (2007).
[19] M. Campiglia, R. Gambini, and J. Pullin, Loop quantization of spherically symmetric midi-superspaces: The interior problem, AIP Conf. Proc. **977**, 52 (2008).
[20] A. Corichi and P. Singh, Loop quantization of the Schwarzschild interior revisited, Classical Quant. Grav. **33**, 055006 (2016).
[21] J. Olmedo, S. Saini, and P. Singh, From black holes to white holes: A quantum gravitational, symmetric bounce, Classical Quant. Grav. **34**, 225011 (2017).

[22] A. Ashtekar, J. Olmedo, and P. Singh, Quantum Transfiguration of Kruskal Black Holes, Phys. Rev. Lett. **121**, 241301 (2018).
[23] A. Ashtekar, J. Olmedo, and P. Singh, Quantum extension of the Kruskal spacetime, Phys. Rev. D **98**, 126003 (2018).
[24] N. Bodendorfer, F. M. Mele, and J. Münch, Effective quantum extended spacetime of polymer Schwarzschild black hole, Classical Quant. Grav. **36**, 195015 (2019).
[25] M. Han and H. Liu, Improved effective dynamics of loop-quantum-gravity black hole and Nariai limit, arXiv: 2012.05729.
[26] W.-C. Gan, N. O. Santos, F.-W. Shu, and A. Wang, Properties of the spherically symmetric polymer black holes, Phys. Rev. D **102**, 124030 (2020).
[27] M. Bojowald and R. Swiderski, Spherically symmetric quantum geometry: Hamiltonian constraint, Classical Quant. Grav. **23**, 2129 (2006).
[28] R. Gambini and J. Pullin, Black Holes in Loop Quantum Gravity: The Complete Space-time, Phys. Rev. Lett. **101**, 161301 (2008).
[29] D.-W. Chiou, W.-T. Ni, and A. Tang, Loop quantization of spherically symmetric midisuperspaces and loop quantum geometry of the maximally extended Schwarzschild spacetime, arXiv:1212.1265.
[30] R. Gambini and J. Pullin, Loop Quantization of the Schwarzschild Black Hole, Phys. Rev. Lett. **110**, 211301 (2013).
[31] R. Gambini, J. Olmedo, and J. Pullin, Quantum black holes in loop quantum gravity, Classical Quant. Grav. **31**, 095009 (2014).
[32] R. Gambini, J. Olmedo, and J. Pullin, Spherically symmetric loop quantum gravity: Analysis of improved dynamics, Classical Quant. Grav. **37**, 205012 (2020).
[33] J. G. Kelly, R. Santacruz, and E. Wilson-Ewing, Effective loop quantum gravity framework for vacuum spherically symmetric spacetimes, Phys. Rev. D **102**, 106024 (2020).
[34] M. Bojowald, R. Goswami, R. Maartens, and P. Singh, Black Hole Mass Threshold from Nonsingular Quantum Gravitational Collapse, Phys. Rev. Lett. **95**, 091302 (2005).
[35] R. Goswami, P. S. Joshi, and P. Singh, Quantum Evaporation of a Naked Singularity, Phys. Rev. Lett. **96**, 031302 (2006).
[36] R. Gambini, J. Pullin, and S. Rastgoo, Quantum scalar field in quantum gravity: The vacuum in the spherically symmetric case, Classical Quant. Grav. **26**, 215011 (2009).
[37] C. Bambi, D. Malafarina, and L. Modesto, Non-singular quantum-inspired gravitational collapse, Phys. Rev. D **88**, 044009 (2013).
[38] Y. Tavakoli, J. Marto, and A. Dapor, Semiclassical dynamics of horizons in spherically symmetric collapse, Int. J. Mod. Phys. D **23**, 1450061 (2014).
[39] F. Benitez, R. Gambini, L. Lehner, S. Liebling, and J. Pullin, Critical Collapse of a Scalar Field in Semiclassical Loop Quantum Gravity, Phys. Rev. Lett. **124**, 071301 (2020).
[40] G. Lemaître, The expanding universe, Annu. Soc. Sci. Bruxelles **53**, 51 (1933).
[41] R. C. Tolman, Effect of inhomogeneity on cosmological models, Proc. Natl. Acad. Sci. U.S.A. **20**, 169 (1934).
[42] H. Bondi, Spherically symmetrical models in general relativity, Mon. Not. R. Astron. Soc. **107**, 410 (1947).
[43] K. Giesel, J. Tambornino, and T. Thiemann, LTB spacetimes in terms of Dirac observables, Classical Quant. Grav. **27**, 105013 (2010).
[44] M. Bojowald, T. Harada, and R. Tibrewala, Lemaitre-Tolman-Bondi collapse from the perspective of loop quantum gravity, Phys. Rev. D **78**, 064057 (2008).
[45] J. G. Kelly, R. Santacruz, and E. Wilson-Ewing, Black hole collapse and bounce in effective loop quantum gravity, Classical Quant. Grav. **38**, 04LT01 (2021).
[46] M. Bojowald, J. D. Reyes, and R. Tibrewala, Non-marginal Lemaitre-Tolman-Bondi-like models with inverse triad corrections from loop quantum gravity, Phys. Rev. D **80**, 084002 (2009).
[47] J. B. Achour, S. Brahma, and J.-P. Uzan, Bouncing compact objects. Part I. Quantum extension of the Oppenheimer-Snyder collapse, J. Cosmol. Astropart. Phys. 03 (2020) 041.
[48] J. B. Achour and J.-P. Uzan, Bouncing compact objects. II. Effective theory of a pulsating Planck star, Phys. Rev. D **102**, 124041 (2020).
[49] K. Liegener and P. Singh, Gauge-invariant bounce from loop quantum gravity, Classical Quant. Grav. **37**, 085015 (2020).
[50] K. Liegener and P. Singh, New loop quantum cosmology modifications from gauge-covariant fluxes, Phys. Rev. D **100**, 124048 (2019).
[51] K. Liegener and P. Singh, Some physical implications of regularization ambiguities in SU(2) gauge-invariant loop quantum cosmology, Phys. Rev. D **100**, 124049 (2019).
[52] T. Thiemann, Quantum spin dynamics (QSD): VII. Symplectic structures and continuum lattice formulations of gauge field theories, Classical Quant. Grav. **18**, 3293 (2001).
[53] C. Kiefer and T. Schmitz, Singularity avoidance for collapsing quantum dust in the Lemaître-Tolman-Bondi model, Phys. Rev. D **99**, 126010 (2019).
[54] J. F. Barbero G., Real Ashtekar variables for Lorentzian signature space times, Phys. Rev. D **51**, 5507 (1995).
[55] G. Immirzi, Real and complex connections for canonical gravity, Classical Quant. Grav. **14**, L177 (1997).
[56] J. Brown and K. V. Kuchar, Dust as a standard of space and time in canonical quantum gravity, Phys. Rev. D **51**, 5600 (1995).
[57] S. A. Hayward, Gravitational energy in spherical symmetry, Phys. Rev. D **53**, 1938 (1996).
[58] A. Wang and Y. Wu, Generalized Vaidya solutions, Gen. Relativ. Gravit. **31**, 107 (1999).
[59] P. S. Joshi and I. H. Dwivedi, Initial data and the end state of spherically symmetric gravitational collapse, Classical Quant. Grav. **16**, 41 (1999).
[60] A. Ashtekar, M. Bojowald, and J. Lewandowski, Mathematical structure of loop quantum cosmology, Adv. Theor. Math. Phys. **7**, 233 (2003).
[61] P. Diener, B. Gupt, and P. Singh, Numerical simulations of a loop quantum cosmos: Robustness of the quantum bounce and the validity of effective dynamics, Classical Quant. Grav. **31**, 105015 (2014).
[62] P. Diener, B. Gupt, M. Megevand, and P. Singh, Numerical evolution of squeezed and non-Gaussian states in loop quantum cosmology, Classical Quant. Grav. **31**, 165006 (2014).

[63] P. Diener, A. Joe, M. Megevand, and P. Singh, Numerical simulations of loop quantum Bianchi-I spacetimes, Classical Quant. Grav. **34**, 094004 (2017).

[64] P. Singh, Glimpses of spacetime beyond the singularities using supercomputers, Comput. Sci. Eng. **20**, 26 (2018).

[65] A. Corichi and P. Singh, Is loop quantization in cosmology unique?, Phys. Rev. D **78**, 024034 (2008).

[66] B.-F. Li and P. Singh, Does the loop quantum μ_o scheme permit black hole formation?, Universe **7**, 406 (2021).